ChemPubSoc Europe

DOI: 10.1002/open.201700121

Open Access ChemistryOPEN Full Papers

Reversible Broad-Spectrum Control of Selective Reflections of Chiral Nematic Phases by Closed-/Open-Type Axially Chiral Azo Dopants

Hiroya Nishikawa,*[a] Daigou Mochizuki,[b] Hiroki Higuchi,[a] Yasushi Okumura,[a] and Hirotsugu Kikuchi*[a]

We demonstrate reversible RGB-color photocontrol of a chiral nematic liquid crystal (N*LC) by using newly synthesized closed- and open-type chiral dopants. The photoswitching elements in the dopants are azobenzene units on axially chiral binaphthyl cores. Owing to *cis–trans* photoisomerization of the azobenzene units, both closed- and open-type compounds showed higher solubility, larger helical twisting power (HTP), and larger changes in HTP than conventional chiral dopants in host LCs. Thus, even at very low dopant concentrations, we successfully controlled the chirality of the induced helical structure of the N*LCs. Consequently, the N*LCs reflected right- and left-handed circularly polarized light (CPL) under a light stimulus. In the N*LCs with closed-type chiral dopants, the RGB-color reflection was reversibly controlled within several seconds. Interestingly, the open-type chiral dopant reversibly inverted CPL with opposite handedness in the near and short-wave IR regions. These novel materials are expected to realize new applications and perspectives in color information and similar technologies.

1. Introduction

In recent years, external dynamic control of molecular self-organized superstructures with unique features has roused significant interest because these structures are applicable to chiral molecular devices. Liquid crystal (LC) materials doped with chiral elements (called chiral nematic LCs, N*LC) generally self-organize into a helical structure with one-dimensional periodicity, which manifests as intrinsic selective Bragg reflection of light.[1] The molecular orientation in the helical structure is very sensitive to external stimuli, such as light,[2–18] electric fields,[13,20–24] and temperature.[13,25–29] Therefore, the helical superstructure of N*LCs is easily controlled by such stimuli. In particular, external stimuli control the chirality variables, that is, the helical pitch length and/or helical sense in N*LCs. Of these external stimuli, light is particularly attractive because it enables remote photocontrol of the chirality of N*LCs. By exploiting the ability of photoswitchable chiral dopants, both spatial and temporal photocontrol becomes possible.

The center wavelength of the selective reflection light (λ_0) is related to the helical pitch (p) as follows [Eq. (1)]:

$$m\lambda_0 = np\cos\phi \quad (1)$$

in which m is the diffraction order, n is the average refractive index of the LC matrix for incident light, and ϕ is the angle of incident light. If unpolarized or linearly polarized light is incident on the N*LC along its helical axis, the N*LC selectively reflects circularly polarized light (CPL) with the same helical handedness. Therefore, when the helical sense of the N*LC is inverted, the handedness of the reflected CPL is also reversed, and opposite-handed CPL is transmitted through the media. The ability of a chiral dopant to twist the nematic director and, therefore, induce a helical structure, is called the helical twisting power (HTP, β). At sufficiently low concentration of a chiral dopant, the HTP is inversely proportional to the helical pitch, given by Equation (2):

$$\beta = (p \cdot c)^{-1} \quad (2)$$

Here, p is the helical pitch of the chiral LC and c is the weight concentration of the chiral dopant in the host LC.

Therefore, reflection wavelength modulation, that is, control of the optical chirality by photoreacting LCs with photoswitchable chiral dopants, is an excellent nanofabrication approach to construct unique photodriven devices for conventional applications, such as tunable LC lasers,[21,28,30] tunable LC color fil-

[a] H. Nishikawa, Dr. H. Higuchi, Dr. Y. Okumura, Prof. H. Kikuchi
Institute for Material Chemistry and Engineering
Kyushu University
6-1 Kasuga-Koen, Kasuga, Fukuoka 816-8580 (Japan)
E-mail: nishikawa@cm.kyushu-u.ac.jp
kikuchi@cm.kyushu-u.ac.jp

[b] D. Mochizuki
Interdisciplinary Graduate School of Engineering Sciences
Kyushu University
6-1 Kasuga-Koen, Kasuga, Fukuoka 816–8580 (Japan)

Supporting Information for this article can be found under: https://doi.org/10.1002/open.201700121.

ters,[31,32] and optically addressed flexible displays without patterned electronics.[18,19]

Azobenzene-tethered chiral dopants undergo reversible *trans–cis* photoisomerization, which plays an important role in photocontrol of the macroscopic helical structure of N*LCs. Although the photocontrol of the helical pitch has been well studied,[4–10] there are only a few reports on the photoinduced helical inversion of N*LCs,[6] possibly because of the small change in HTP (ΔHTP) across HTP = 0 before and after the photochemical reaction. Owing to the low HTP values of the dopants, reversible photocontrol of the reflected color and/or the handedness of the reflected CPL over the entire visible range has required high concentrations of the chiral dopants (5.0–23 wt%) in the host LCs.[4–10] If a chiral dopant has a large intrinsic HTP, its concentration can be significantly reduced. Chiral dopants with large HTP values at low concentration would simplify the fabrication of CPL materials and offer low-cost photocontrol of the CPL properties without losing the properties of the host LCs (e.g., the high phase-transition temperatures of the LCs).

Herein we demonstrate the reversible photocontrol of selective reflection bands over various spectral ranges (UV, Vis, NIR, and short-wave IR (SWIR)) by doping LCs with closed- and open-type chiral elements. Interestingly, the N*LC induced by compound **3** rapidly reversed the RGB color at low dopant concentration to give high-resolution images without decreased contrast. Equally notably, the N*LC induced by compound **7** not only photocontrolled the reflection band from the UV through Vis to the IR/SWIR regions, but also inverted the handedness of the reflected CPL over the IR/SWIR region under light stimuli. This reversible broad tuning with handedness inversion of the reflected CPL has unprecedented utility and great potential.

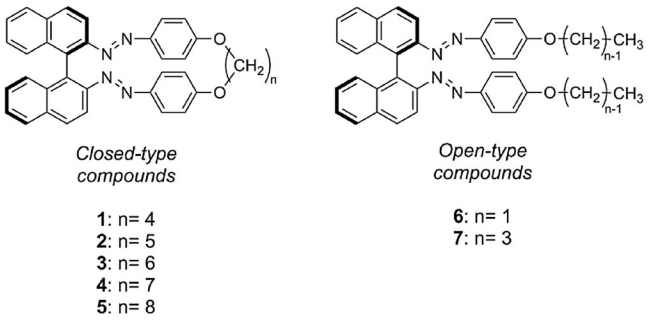

Figure 1. Chemical structures of closed- and open-type binaphthyl chiral dopants with two azobenzene moieties and various alkyl chain lengths: closed-type (**1**–**5**; $n = 4$, 5, 6, 7, 8) and open-type (**6**, **7**; $n = 1$, 3) dopants with the (*R*) configuration.

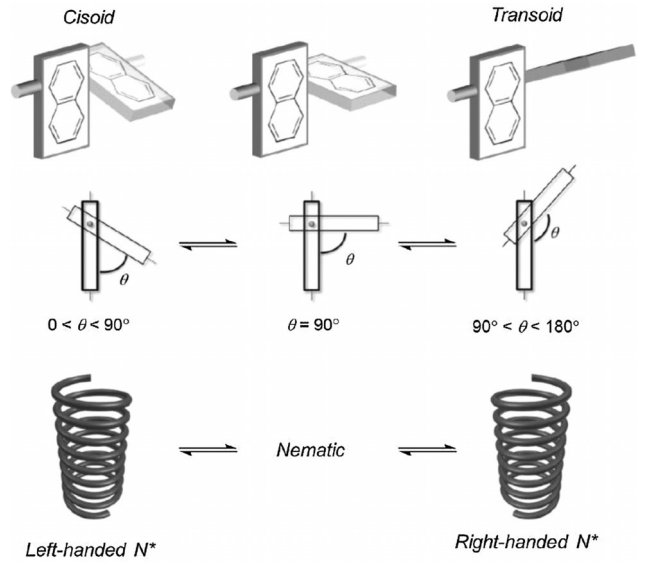

Figure 2. Relationship between the (*R*)-binaphthyl core and the induced helical direction of N*LCs.

2. Results and Discussion

2.1. Molecular Design, Synthesis, and Spectral Characteristics

We designed structurally related molecules with two azobenzene units that can undergo *trans–cis* photoisomerization. We synthesized two types of closed/open dopants (**1**–**5** and **6**–**7**) as photoswitchable chiral dopants. The dopants are comprised of axially chiral binaphthyl with azobenzene units as the photoswitching trigger (see Figure 1). Of the three types of generation elements in chiral dopants (point, plane, and axial), we selected axially chiral binaphthalene because it induces a short-pitch helical structure in the nematic LC. In other words, binaphthalene exhibits high HTP. As shown in Figure 2, the HTP of binaphthalene is governed by its molecular conformation. By convention, when the dihedral angle (θ) between the two naphthalene rings of (*R*)-binaphthalene is $0 < \theta < 90°$, the conformation is *cisoid*. The other conformation, $90 < \theta < 180°$, is called *transoid*. The HTP is maximized at $\theta \approx 45$ or 135° and negligible at $\theta \approx 90°$.[28–30] Moreover, the *transoid* and *cisoid* conformations of (*R*)-binaphthalene induce right- and left-handed N*LCs, respectively (see Figure 2).[31,32] In closed-type dopants **1**–**5**, the alkyl bridge part rigidifies the binaphthyl core and limits the rotation around the C1–C1′ axis. Therefore, the closed-type series should be inevitably fixed in the *transoid* conformation. Open-type dopants **6** and **7** lack the alkyl bridge part, so rotation around the C1–C1′ axis is relatively free, which enables a dramatic structural change. Consequently, a light stimulus can induce a large chirality change in the N*LCs.

Figure 3a and b show the UV/Vis absorption and circular dichroism (CD) spectra, respectively, of closed-type **3** and open-type **7** dissolved in acetonitrile (MeCN). In Figure 3a, the two main absorption regions at $\lambda < 250$ nm and between 250 and 320 nm characterize the naphthalene chromophores in the compounds. The absorptions at $\lambda < 250$ nm were attributed to ^1B_b (long-axis polarization), whereas the absorption at $\lambda = 250$ to 320 nm is due to the ^1L_b transition (long-axis polarization) and ^1L_a transition (short-axis polarization) of the naphthalene chromophores.[38–40] The large peak at $\lambda = 320$ to 430 nm in the spectra of both compounds (extinction coefficient $\varepsilon_{max} = 45 \times 10^3$ (**3**) and 59×10^3 L mol^{-1} cm^{-1} (**7**)) and the weak peak at $\lambda = 430$ to 560 nm arise from the $\pi \rightarrow \pi^*$ and $n \rightarrow \pi^*$ transitions of

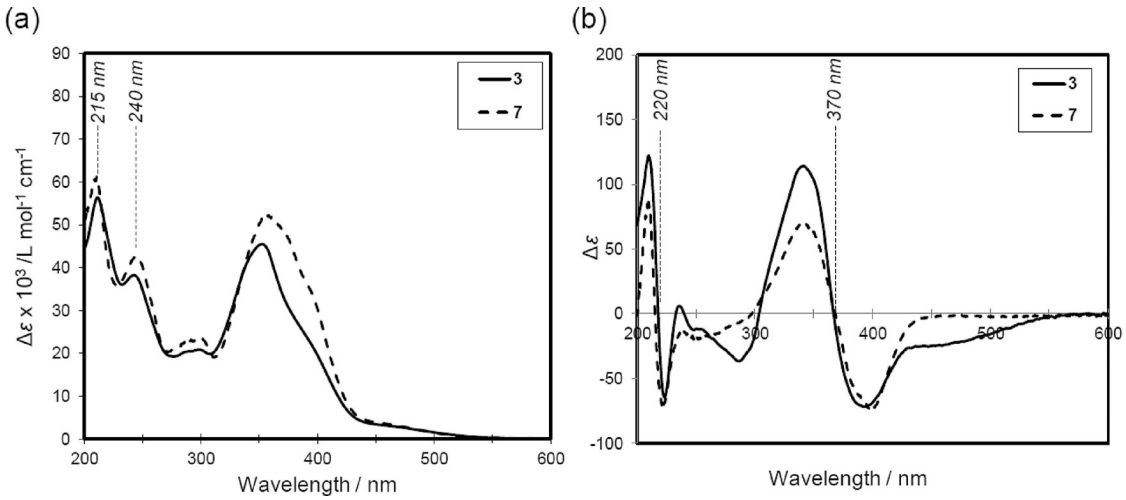

Figure 3. a) UV/Vis and b) CD spectra of dopants **3** and **7** in MeCN (**3**: 2.3×10^{-5} M, **7**: 2.1×10^{-5} M).

the azobenzene units, respectively. Below $\lambda=250$ nm, the absorptions are clearly split into two peaks at approximately $\lambda=$ 215 and 240 nm, which indicates a dihedral angle of less than 90° between the two naphthalene rings. This result is supported by Bari et al., who simulated 1,1′-binaphtyl by using DeVoe's approach and observed two absorption bands below $\theta=90°$, but only one band at $\theta=90°$.[39,40] Interestingly, for the intense absorption at around $\lambda=360$ nm, due to the $\pi\rightarrow\pi^*$ transition, the ε_{max} value of **3** and **7** was higher than that of common molecules with an azobenzene unit. The data and the large absorption band of the chiral dopants are discussed in the Supporting Information.

Similarly, two distinct CD bands with opposite signs at around $\lambda=220$ and 370 nm were observed (Figure 3b). The negative exciton couplet at around $\lambda=220$ and 370 nm is due to the ^1B_b transition of the naphthalene parts and the excitations of the azobenzene moieties, respectively. Similar UV/Vis and CD spectra have been observed in another compound (see Figures S1 and S2 in the Supporting Information).

2.2. Photoisomerization in Solution

To study the isomerization behavior of compounds **1**–**7**, we measured the UV/Vis spectra of the closed- and open-type dopants in acetonitrile under alternating irradiation at $\lambda=400$ ($I=1.0$ mW cm^{-2}) and 460 nm ($I=1.0$ mW cm^{-2}). The UV/Vis and CD spectral changes of **3** and **7** in MeCN are shown in Figure 4 (data for the other compounds are summarized in Figures S1 and S2). Under light irradiation at $\lambda=400$ nm, the UV/Vis signal of the $\pi\rightarrow\pi^*$ transition band of the *trans* azobenzene isomer ($\lambda\approx360$ nm) decreased whereas the band corresponding to the $n\rightarrow\pi^*$ transitions of the *cis* azobenzene isomer ($\lambda=\approx460$ nm) slightly increased (Figure 4a, b). The photostationary state at $\lambda=400$ nm (PSS_{400}) was attained within 2 min. Under light irradiation at $\lambda=460$ nm, the absorption spectral changes were elevated and the photostationary state at $\lambda=460$ nm (PSS_{460}) was reached within 3 min (Figure 4a, b). The CD spectral changes in **3** and **7** after photoisomerization were investigated by using CD spectroscopy (see Figure 4c, d). The changes in the intensity of the CD signals indicate the effect of *trans–cis* isomerization on the structural change of the chiral dopants (Figure 4c, d). The intensity of the negative exciton couplet at around $\lambda=220$ nm decreased under irradiation at $\lambda=400$ nm and recovered under irradiation at $\lambda=460$ nm. This indicates a *trans–cis* isomerization that changed the dihedral angle of the binaphthyl unit in the molecule. Under irradiation at both $\lambda=400$ and 460 nm, the CD spectra changed fully within a few minutes. The negative exciton couplet at around $\lambda=360$ nm, assigned to the $\pi\rightarrow\pi^*$ transition of *trans* azobenzene units in **3** and **7**, appeared with reduced intensity at around $\lambda=370$ nm under $\lambda=400$ nm irradiation. Additionally, a positive CD signal derived from the $n\rightarrow\pi^*$ transition of *cis* azobenzene appeared under illumination at $\lambda=400$ nm. After subsequent irradiation at $\lambda=460$ nm, the negative exciton couplet was restored and the positive one diminished. These results can be ascribed to isomerization of the azobenzene moieties from *trans* to *cis* and vice versa. The other chiral dopants showed similar behavior in MeCN.

2.3. HTP Measurements and Optical Chirality Control

To evaluate whether the chiral dopants could provide chirality to achiral N*LC molecules, we measured the temperature dependence of the HTP values of compounds **1**–**7** in a nematic LC host, 5CB/JC-1041XX (1:1 w/w). The HTP values were calculated by using Equation (2). The magnitude of p in the induced N* phase was estimated by using Cano's wedge method. The helical sense of N* in the chiral dopants was determined by using the contact method with a known left-handed N*LC (cholesteryl oleyl carbonate) as the standard.[41] The sign of the HTP indicates the helical sense of the induced N*LCs. Specifically, a positive and negative HTP means that the induced N* phase is a right- and left-handed helix, respectively.

Figure 5a shows the HTPs of compounds **1**–**7** (0.5 wt%) in the host nematic mixture as the temperature was increased from 25 to 55 °C. During the heating process, the LCs exhibited

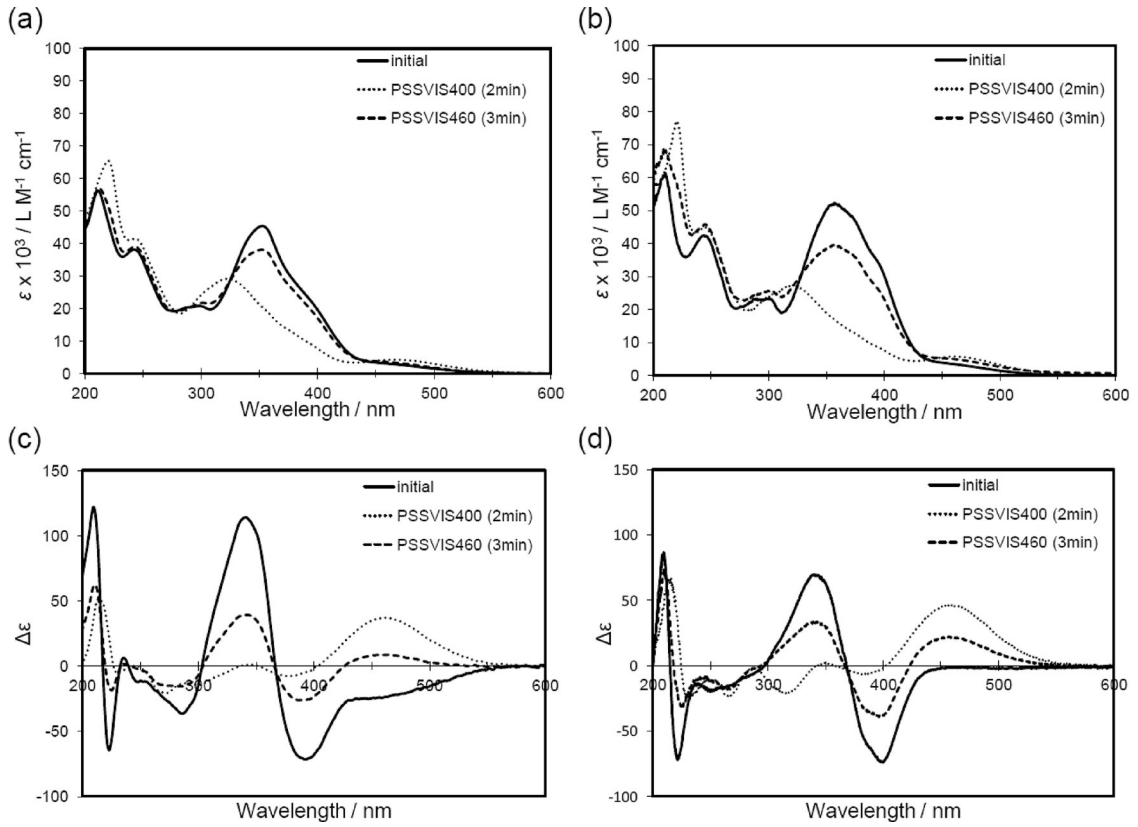

Figure 4. UV/Vis spectral changes for a) **3** and b) **7** in MeCN (**3**: 2.3×10^{-5} M, **7**: 2.1×10^{-5} M) under visible light irradiation at $\lambda=400$ nm ($I=1.0$ mW cm^{-2}) followed by $\lambda=460$ nm ($I=1.0$ mW cm^{-2}) at ambient temperature. CD spectral changes for c) **3** and d) **7** under the same UV/Vis spectroscopy conditions. Solid lines denote the initial state. Dotted and dashed lines represent the photostationary states at $\lambda=400$ and 460 nm, respectively.

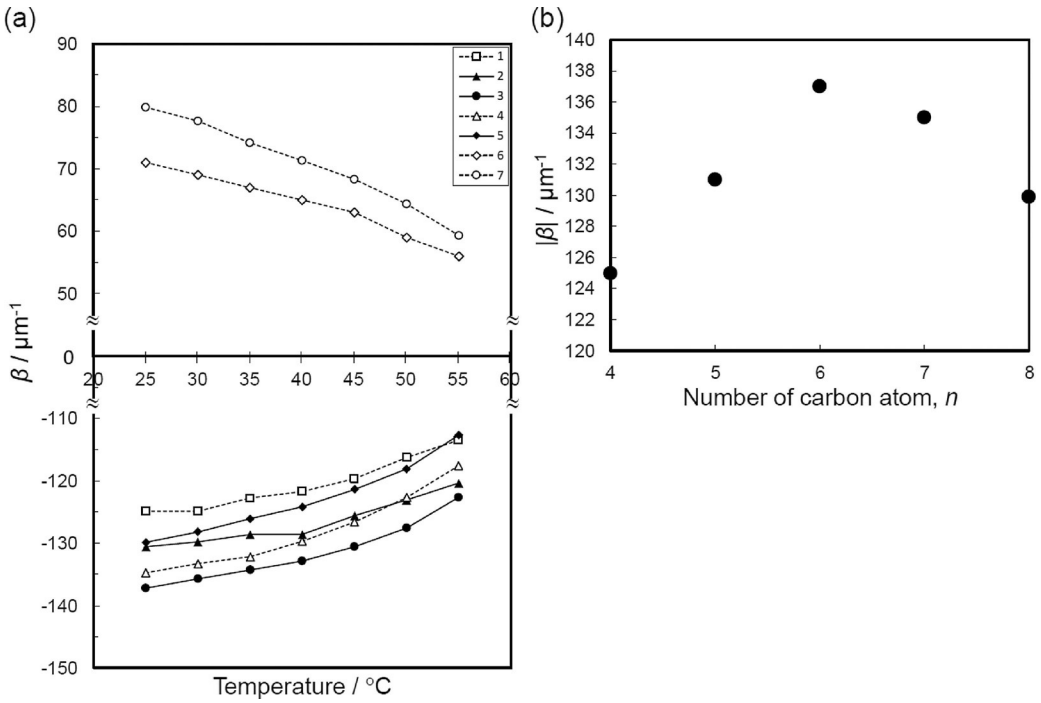

Figure 5. HTP values for chiral dopants **1**–**7** (0.5 wt%) in their nematic host, 5CB:JC-1041XX (1:1 w/w). a) Temperature dependence of HTP between 25 and 55 °C. b) Relationship between |HTP| and the number of carbon atoms in the bridge part of compounds **1**–**5** at 25 °C.

a phase transition from the N* phase to an isotropic phase at $T_c = 56.8\,^{\circ}C$, regardless of the dopant. The absolute value of HTP, denoted |HTP|, increased as the temperature decreased for compounds **1**–**7** and the results are given in Table 1. Over

Table 1. Helical twisting powers (β) of the closed-type series **1**–**5** and the open-type series **6**, **7** in their nematic LC host (5CB:JC-1041XX (1:1 w/w)) at 25 °C, measured by using Cano's wedge method and the change in the HTP value under visible-light irradiation.

Dopant	β (wt%) [μm^{-1}]			$\lvert\Delta\beta\rvert$ (wt%)[a]	$\lvert\Delta\beta/\beta_{initial}\rvert$ [b]
	initial	PSS_{400}	PSS_{460}	[μm^{-1}]	[%]
1	−125	−88	−114	37	30
2	−131	−82	−107	49	38
3	−137	−73	−109	64	43
4	−135	−68	−103	67	50
5	−130	−54	−96	76	59
6	+72	−9.4	+34	81	113
7	+80	−6.6	+25	87	109

[a] $|\Delta\beta| = |\beta_{PSS400} - \beta_{initial}|$. [b] Percentage change in β.

the same temperature range, the |HTP| values were larger in compounds **1**–**5** than in compounds **6** and **7**. This indicates that the binaphthyl structure differs between chiral dopants **1**–**5** and dopants **6** and **7**. Because the dihedral angle of compounds **1**–**5** is fixed by the alkyl-chain bridge, these compounds should impose high chirality on the host LC. Interestingly, we found that the β (molar HTP) values of compounds **1**–**5** were five times higher than in bridged binaphthyl derivatives without the azobenzene units, which were previously synthesized by our group.[42] For example, the maximum β value of our previous closed binaphthalene was 53 μm^{-1} at 6.8 °C below the clearing point (i.e. the LC phase-isotropic liquid transition temperature, T_c−6.8 °C), whereas that of compounds **1**–**5** was approximately 260 μm^{-1} (T_c−6.8 °C). In terms of their |HTP| values, compounds **1**–**5** compete with closed- and open-type binaphthyl derivatives reported in earlier studies.[3–8,10,13–17] The host LCs might receive chirality not only through the binaphthyl cores of the dopants but also through the azobenzene units, which are directly connected to the binaphthyl core. Therefore, the azobenzene units in the chiral dopants should effectively amplify the HTPs. This hypothesis is supported by the CD spectra of the chiral dopants (see Figure 3b and Figures S1 and S2), in which the UV/Vis spectra and bisignate CD signals derived from the two azobenzene group are remarkably amplified at around $\lambda = 360$ nm. We also evaluated the intrinsic temperature dependence of HTP in compounds **1**–**7** (see Table S1).

Next, we investigated the relationship between the number of alkyl carbon atoms in the bridge part of the chiral dopants and the corresponding |HTP| values (see Figure 5b). The |HTP| values at 25 °C for compounds **1**–**5** were 125, 131, 137, 135m and 130 μm^{-1}, respectively. Note that compounds **1** and **3** delivered the lowest and highest |HTP| values, respectively, at this temperature. The |HTP| value increased monotonically as the number of carbon atoms in the bridge part increased from $n = 4$ to 6, then decreased from $n = 7$ to 8. Therefore, we infer that the dihedral angle of the bridged dopant approached 45° when $n = 6$.

We then investigated the effect of photoisomerization of the chiral dopants on the corresponding HTP values and the helical direction induced in the N*LC. When irradiated at $\lambda = 400$ and 460 nm, the pitch of the N*LC changed under the *trans*–*cis* photoisomerization of the chiral dopants. This change can be measured as a change in the distance between the Cano lines in a wedge cell by using a polarized optical microscope. The HTP values of the chiral dopants before and after photoisomerization were calculated by using Equation (1). The helical direction of the N*LCs doped with compounds **1**–**7** at the PSS_{400} and PSS_{460} were determined by using the contact method. The results are also summarized in Table 1 (see also Figure S4). In the initial state, the helical senses of the N*LCs with closed- and open-type dopants were left-handed (− sign) and right-handed (+ sign), respectively. In the N^* phase of LCs with dopants **1**–**5** (0.5 wt%), the Cano lines considerably widened under light irradiation at $\lambda = 400$ nm ($I = 1.0\ mW\,cm^{-2}$). Within 5 min, the compounds reached the PSS_{400} and the Cano lines remained at constant width. For the closed-type derivatives, the HTP at PSS_{400} decreased as the number of carbon atoms on the bridge part increased. Photoisomerization from *trans* to *cis* disrupts the linearity and coplanarity between the naphthalene ring and an azobenzene unit. Consequently, the major chiral inducer is the binaphthyl backbone, and the HTP values at PSS_{400} decrease to those of binaphthyl cores without the azobenzene groups. Under irradiation at $\lambda = 400$ nm, the helical pitch was enlarged by the structural change in the chiral dopant during the *trans* to *cis* isomerization of azobenzene. Subsequent irradiation at $\lambda = 460$ nm ($I = 1.0\ mW\,cm^{-2}$) mostly restored the pitch to the PSS_{460} level within 5 min, and the chiral dopant structure was re-altered by the *trans*–*cis* photoisomerization. We also estimated the recovery rates of compounds **1**–**5** at PSS_{460} ($|HTP_{PSS460}/HTP_{initial}|$) and obtained values of 91, 82, 80, 76, and 74%, respectively.

The helical sense of the N* phase induced by compounds **1**–**5** was unchanged after sequential irradiation at $\lambda = 400$ and 460 nm. This indicates that although photoisomerization altered the structure of the closed-type series, the *cisoid* conformation at PSS_{400} and PSS_{460} was preserved by the strictly restricted rotation around the chiral axis of the binaphthyl core, which was fixed by the bridge part. Conversely, irradiation at $\lambda = 400$ nm elongated the helical pitch of the N* phase induced by compounds **6** and **7** in the host LC, which reflected the decreased HTP value during *trans*–*cis* photoisomerization. In the optical microscopy measurements, the distance between the Cano lines considerably lengthened and eventually disappeared from the field of view before reappearing. The PSS_{400} was achieved within 5 min. Interestingly, the helical direction induced by compounds **6** and **7** at PSS_{400} was opposite to that of the initial state. This suggests that compounds **6** and **7** adopted the *transoid* conformation, whereas they adopted the *cisoid* conformation after photoisomerization. In addition, the *transoid* conformation of compounds **6** and **7** in the initial state (with θ close to 135°) achieved a relatively high HTP value. However, after photoisomerization, the HTP values of

compounds **6** and **7** decreased as the photoinduced *cisoid* conformation possibly became quasi-orthogonal ($\theta \approx 90°$)[43] Under irradiation at $\lambda = 460$ nm, the helical pitch and the sense partly returned to the initial state within 5 min. The $|HTP_{PSS460}/HTP_{initial}|$ values of **6** and **7** were 47 and 32%, respectively. As expected, the open-type molecule can control the helical direction before and after isomerization.

The magnitude of the change in HTP between the initial state and the PSS_{400} was calculated from the ratio of the difference between the HTP values before and after isomerization and the initial HTP value, $|\Delta\beta/\beta_{initial}|$ (expressed as a percentage). Of compounds **1**–**5**, the $|\Delta\beta/\beta_{initial}|$ value was lowest for compound **1** (30%), midrange for compound **3** (43%, although this compound exhibited the highest HTP value in the initial state), and highest for compound **5** (59%). The $|\Delta\beta/\beta_{initial}|$ values increased as the length of the bridged part increased (i.e. from **1** to **5**). This suggests that the short bridge in compound **1** disabled significant changes in the steric structure. Thus, compound **1** is structurally more rigid and conformationally more restricted than compounds **2**–**5** and its $|\Delta\beta/\beta_{initial}|$ value is low. In contrast, owing to the relatively long alkyl chain in its bridge part, compound **5** could flexibly and highly deform its structure during isomerization, so its $|\Delta\beta/\beta_{initial}|$ value was high. The $|\Delta\beta/\beta_{initial}|$ values of compounds **6** and **7** were 113 and 109%, respectively. The $|\Delta\beta/\beta_{initial}|$ values that exceed 100% indicated a helical inversion in the N*LCs. In this case, although the photoisomerization reversed the handedness from *trans* to *cis*, the induced helical pitch was larger at the PSS_{400} than in the initial state. Thus, compounds **6** and **7** can switch the sign of the HTP value across the nematic phase transition; however, the |HTP| value was smaller at the PSS_{400} than in the initial state. In summary, compounds **3**–**5** with long alkyl bridges delivered high |ΔHTP| ($\gtrsim 60$) and high |ΔHTP/HTP| ($\gtrsim 40$) values, which indicated that these materials can drastically change and control the induced chirality of their host LC under light stimulus. In compounds **6** and **7**, the |ΔHTP| and |ΔHTP/HTP| values exceeded 80 and 100, respectively, which confirmed that these compounds can reversibly and controllably invert the induced helical sense of the N*LCs by photoisomerization.

2.4. Reversible Photocontrol of Reflection Colors over a Wide Spectral Region

To demonstrate the reversible photocontrol of selected reflection colors, we doped the host LC mixture with closed- and open-type chiral dopants (**3** and **7**, respectively). These dopants were chosen for their favorable abilities that is, high initial HTP, high $|\Delta\beta/\beta_{initial}|$ yield by photoisomerization and/or photoinducible helical inversion. The mixed solutions (3.3 wt% **3**/LC and 7.0 wt% **7**/LC) were injected into a cell coated with polyimide (10 μm thick). To photocontrol the reflection colors selectively, we first recorded the UV/Vis spectral changes in both samples during light irradiation at $\lambda = 400$ and 460 nm ($I = 1.0$ mW cm^{-2}). Figure 6 shows the notch bands of **3**/LC and **7**/LC, which show changes in the selected reflection bands. The **3**/LC system generated no reflection band in the initial state (Figure 6a), which indicated a reflection band below $\lambda = 400$ nm (unfortunately, in the range below $\lambda = 400$ nm, the absorption band of **3**/LC overlapped that of the coated polyimide (composed of π-conjugated aromatic rings), so the spectrum could not be recorded). Under irradiation at $\lambda = 400$ nm for 120 s, the selective reflection band shifted toward longer wavelength until the PSS_{400} was reached. During this process, the reflection color changed from violet to red ($\lambda_0 \approx 700$ nm). In contrast, subsequent irradiation at $\lambda = 460$ nm for 180 s reversibly altered the color reflection from red to blue ($\lambda_0 \approx 450$ nm; see Figure 6b). Figure 7a shows the corresponding variety of reflection colors resulting from the reversible phototuning of **3**/LC under irradiation at $\lambda = 400$ and 460 nm at different times. Even at relatively weak intensity ($I = 1.0$ mW cm^{-2}), the irradiation induced strong and reversible multicolor changes over the entire visible-light region.

As mentioned above and in Section 2.3, compound **3** photocontrolled the helical pitch of the induced N* with left-handedness. Therefore, **3**/LC can potentially photocontrol the reflection color over the entire visible region with left-handed CPL (CPL_{LH}). To evaluate the CPL handedness of the reflection colors, we performed polarized optical microscope (POM) observations filtered through left- and right-handed CPL films. Figure 7c and d show the reflection color changes under light irradiation at $\lambda = 400$ and 460 nm, respectively. The left and right photographs in each panel are POM images observed through left- and right-handed CPL films, respectively. During alternating irradiation at $\lambda = 400$ and 460 nm (Figure 7c and d), reflection colors were observed through the left-handed CPL film, but the right-handed CPL film remained dark. This indicates that CPL_{LH} was selectively reflected from the N*LC doped with compound **3**. This handedness of the selectively reflected CPL agrees with the handedness of the induced N*LC.

We also demonstrated tuning of the reflected RGB color under LED light irradiation at $\lambda = 405$ and 470 nm ($I = 7.9$ mW cm^{-2}). Quick (within 9 s) and reversible phototuning was achieved across the RGB region (Figure 8). Interestingly, even when doped with even small amounts of compound **3**, the host LC reversibly phototuned the RGB-color reflection within several seconds. At low concentrations (3.3 wt% in **3**/LC), self-reflection is less likely to reduce the coloration and contrast of the reflected RGB color. Furthermore, there was no detrimental effect to the reflection intensity or width of reflection bands, unlike in electrocontrol of color reflection.

Under irradiation at $\lambda = 400$ nm ($I = 1.0$ mW cm^{-2}) for 90 s, the reflection color of **3**/LC changed from violet to red ($\lambda_0 \approx 750$ nm; see Figure 6c and Figure 7b). Further photoirradiation caused a shift in the reflection band toward the NIR region (i.e. up to $\lambda = 1000$ nm). After continuous photoirradiation for 250 s, the reflection spectrum shifted to over $\lambda = 2400$ nm (into the SWIR region). Unfortunately, no peaks over $\lambda = 2400$ nm were detected in our experimental setup. In the NIR and SWIR regions, the intensity of the reflection band decreased and broadened as the helical pitch elongated. To overcome this problem, we could use a thicker cell with a cell gap that exceeded 10 μm.[5] After subsequent light irradiation at $\lambda = 460$ nm for 360 s, the reflection band reversibly shifted

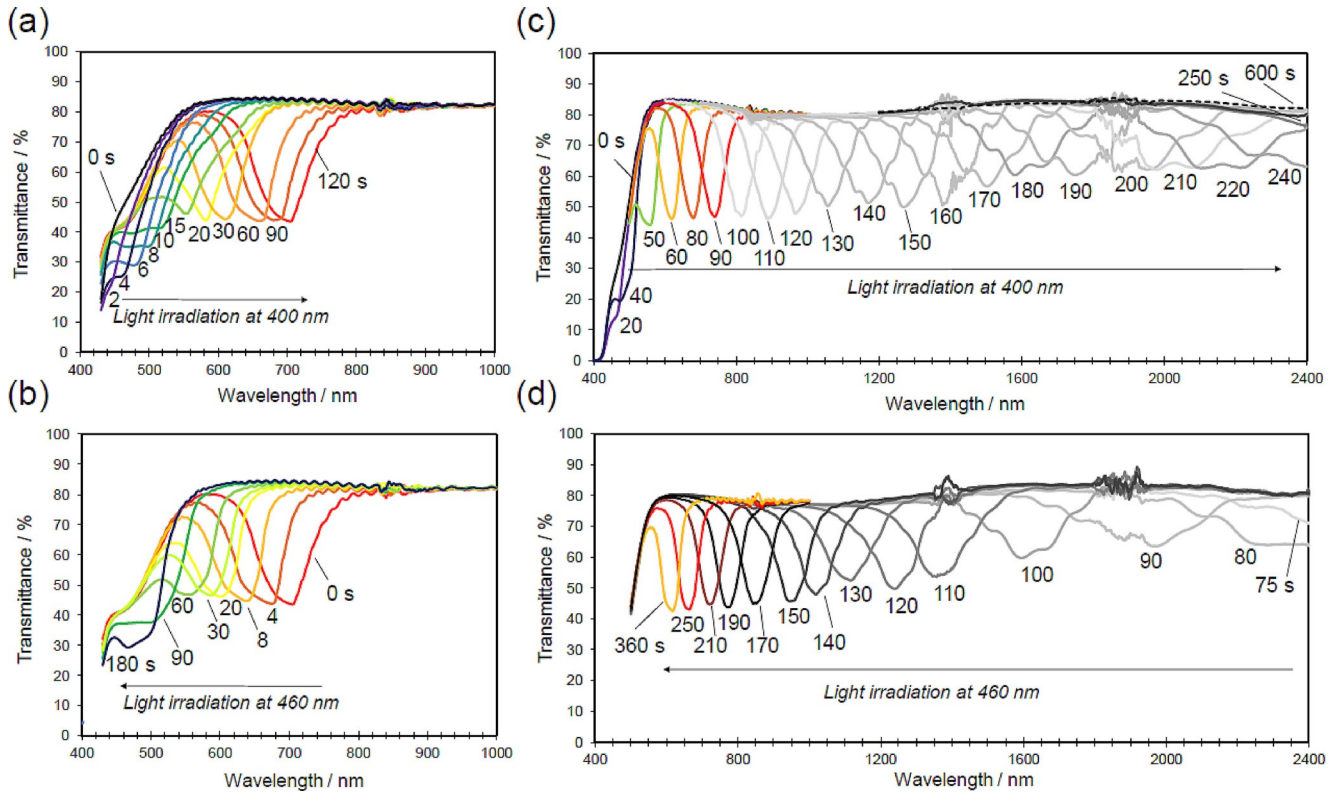

Figure 6. Phototuning of selective reflection spectra of a, b) closed- and c, d) open-type chiral dopants in host LCs in a planar cell (cell gap: 10 μm) at room temperature under visible light irradiation at 400 nm (top) and 460 nm (bottom). The cell was injected with **3**/LC (3.3 wt%) or **7**/LC (7.0 wt%) and irradiated at $\lambda = 400$ (a, c) and 460 nm (b, d). The black dotted line in (c) is the spectrum after irradiation at $\lambda = 400$ nm for 600 s (after 600 s, the helical inversion of the induced N* was complete). All spectra curves were smoothed by using an adjacent averaging method (Origin Pro 8).

from over $\lambda = 2400$ nm to $\lambda \approx 620$ nm (Figure 6d and Figure 7b). As mentioned in Section 2.3, light irradiation reversed the HTP sign of the N*LC doped with compound **7** (**7**/LC). Therefore, the CPL handedness of **7**/LC should be also inverted through *trans–cis* photoisomerization. To determine the irradiation time that completely reversed the handedness of the induced N*LCs, we performed POM observations under light irradiation and the experimental conditions in Figure 6 (see Figure S6 in the Supporting Information). After irradiation for 460 s at $\lambda = 400$ nm, the handedness of the induced N*LCs was completely converted from right to left via the transient N phase. Based on Figure 6c, such a long irradiation time should induce a long-pitched N*LC in the NIR and SWIR regions. Therefore, the handedness of the induced N* and the corresponding handedness of the CPL should be inverted in the NIR/SWIR region.

Finally, we attempted to assign the CPL handedness of the reflection colors of the induced N*LC (7.0 wt% **7**/LC) over the entire visible region. Again, we equipped a POM with left- and right-handed CPL films and applied two light sources ($\lambda = 400$ nm, $I = 1.0$ mW cm^{-2}; $\lambda = 600$ nm, $I = 6.0$ mW cm^{-2}). Irradiation at $\lambda = 600$ nm promoted the photo back reaction. As shown in Figure 7e and f, the behavior was reversed from that of **3**/LC, namely, the POM images through the left-handed CPL film remained dark under irradiation at $\lambda = 400$ nm (Figure 7e) and showed reflection colors through the right-handed CPL film (Figure 7f). Thus, the CPL handedness of the reflection color should be assigned to right-handedness.

3. Conclusions

We designed and synthesized two types of photodriven chiral dopants. The two groups differed in the presence or absence of a bridge over the axial chiral source (the binaphthyl skeleton). Both closed- (**1**–**5**) and open-type (**6**, **7**) chiral dopants exhibited high and rapid photoswitching ability with chiroptical properties in an isotropic solution and in LC media. In the initial state, the closed-type derivatives adopted the *cisoid* conformation in both media, whereas their open-type counterparts adopted the *transoid* and *cisoid* conformation in the organic solution and LC media, respectively. In their host LCs, dopants **1**–**5** exhibited high HTP value in the initial state and a large change in HTP with the same sign (−) under light stimuli. The $\beta_{initial}$ value was highest for compound **3**. In open-type derivatives **6** and **7**, photoswitching reversibly switched the helical structure in N*LC under light stimuli. Even at low concentrations, dopants **3** and **7** reversibly controlled the multicolored reflection of CPL with left- or right-handedness under a light stimulus. By inducing a helical structure in the host N*LC, the dopants enabled reflection over the entire visible region. Moreover, **3**/LC achieved rapid (within several seconds) reversible tuning of the RGB-color reflection. Additionally, the CPL

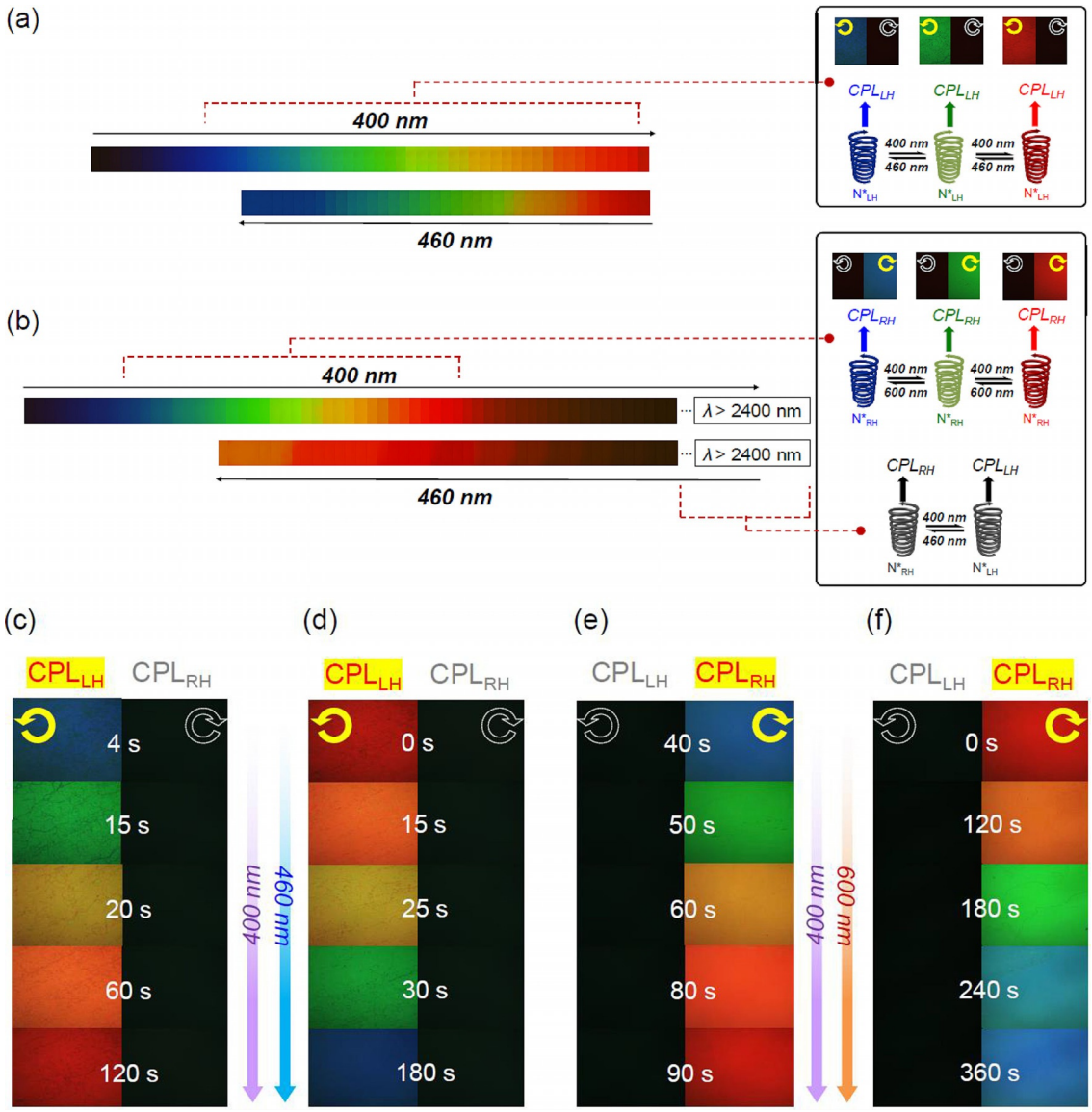

Figure 7. Reversible variable color changes for a) **3**/LC (3.3 wt%) and b) **7**/LC (7.0 wt%) in a planar cell (cell gap: 10 μm) under irradiation at $\lambda = 400$ and 460 nm ($I = 1.0$ mW cm^{-2}) at different times (1–2 s intervals). All images were captured by using a POM in reflection mode. The CPL handedness of the reflection colors was assigned by using left- and right-handed CPL films in the POM observations. N^*_{LH} and N^*_{RH} denote left- and right-handed N* phases, respectively. System **3**/LC (3.3 wt%) displays reversible wide-ranging color changes across the RGB-reflection region of the left-handed CPL (CPL_{LH}). In contrast, **7**/LC (7.0 wt%) showed reversible phototuning of the reflection colors across the RGB-reflection region of the right-handed CPL (CPL_{RH}). Under irradiation alternated between $\lambda = 400$ and 460 nm, the tuning reflection band reversibly switched between CPL_{RH} and CPL_{LH} in the NIR and SWIR regions. Photocontrol of selective reflections of c,d) CPL_{LH} and e,f) CPL_{RH} over the entire visible region under irradiation alternated between $\lambda = 400/460$ or 400/600 nm light, respectively ($\lambda = 400$, 460 nm: $I = 1.0$ mW cm^{-2}; $\lambda = 600$ nm: $I = 6.0$ mW cm^{-2}).

handedness of reflection bands of **7**/LC (in which **7** induced the handedness of the reflected CPL) were reversibly inverted over the NIR and SWIR regions. Thus, both materials are expected to benefit color information technology and to open new perspectives for cutting-edge future applications.

Experimental Section

General Procedures

A nematic LC mixture, JC-1041XX (JNC Co., $\Delta n = 0.142$, $\Delta\varepsilon = 5.7$ at 25 °C) was used as the host LC. All chemical products to synthesize the chiral dopants and solvents were purchased from commercial suppliers and used without further purification. Column chromatography was carried out on SiO_2 60 N (particle size 0.063–0.210 mm; Kanto Chemical Co.). Thin-layer chromatography was performed on TLC silica gel 60 F_{254} glass plates (Merck). ^{1}H and ^{13}C NMR spectra were recorded at 25 °C in $CDCl_3$ as a solvent by using a JEOL JNM-LA400 (400 MHz) instrument and trimethylsilane as the initial standard. Mass spectra (MS) and elemental analyses were obtained from the Service Center at Kyushu University. UV/Vis and CD spectra were recorded in MeCN by using an UV/VIS/NIR spectrophotometer (SHIMADZU, UV-3150) and spectropolarimeter (JASCO Co., J-720W), respectively. Photoisomerization was conducted by using visible light from a Xenon light source (300 W, ASAHI

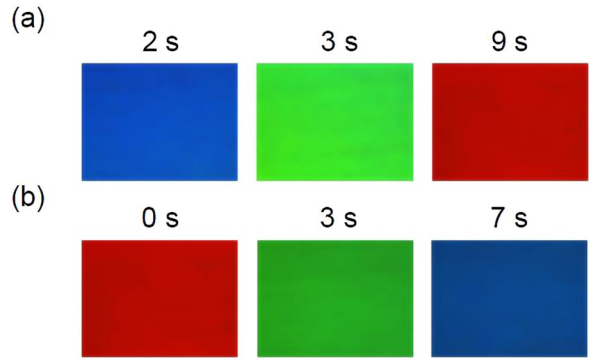

Figure 8. Reversible dynamic changes in blue, green, and red reflections induced by **3**/LC (3.3 wt%) in a planar cell (cell gap: 10 μm) under LED light irradiation at a) $\lambda = 405$ nm ($I = 7.9$ mW cm^{-2}) and b) $\lambda = 470$ nm ($I = 7.9$ mW cm^{-2}) at different times. All images were taken by using a POM in reflection mode.

SPECTRA Co.) through band-pass filters ($\lambda = 400$, 460, and 600 nm, ASAHI SPECTRA Co.). Microscopic analysis was carried out by using a Nikon ECLIPSE E600 POL optical microscope.

Materials

Compounds **1**–**7** were synthesized by an azocoupling reaction of (*R*)-(−)-1,1′-binaphthli-2,2′-diamine with phenol followed by a condensation reaction with the corresponding dibromoalkane. In the case of closed-type derivatives, the condensation reaction was performed under pseudo high-dilution conditions. The resulting crude products were purified by using column chromatography on silica gel with hexane/dichloromethane (1:1 v/v) as the eluent. All target compounds were identified by using ^{1}H and ^{13}C NMR spectral studies, fast atom bombardment mass spectrometry (FABMS), and elemental analysis (EA).

Azo Precursor

The precursor of closed- and open-type series, **Azo precursor**, was synthesized according to a previous paper by Pieraccini et al.[45] Spectroscopic characterization of the obtained product agreed with literature data.[45]

Compound 1

Azo precursor (500 mg, 1.01 mmol), K_2CO_3 (559 mg, 4.04 mmol), and DMF (500 mL) were added to a three-neck flask (3 L). The mixture was stirred for 1 h at RT and then warmed to 80 °C. A solution of 1,4-dibromobutane (262 mg, 1.21 mmol) in DMF (667 mL) was added over 6 d with stirring. After distilled water was added to the resulting mixture to dissolve residual K_2CO_3, the solution was extracted with Et_2O, washed with distilled water, dried over Na_2SO_4, filtered, and then evaporated. The residue was purified by using column chromatography on silica gel with hexane/DCM (1:1) as the eluent to give **1** as an orange amorphous solid (yield: 133 mg, 6%). ^{1}H NMR (400 MHz, $CDCl_3$, TMS): $\delta = 1.40$ (m, 2H), 2.18 (m, 2H), 4.01 (m, 2H), 4.49 (m, 2H), 6.50 (br s, 4H), 7.22–7.25 (m, 6H), 7.26–7.31 (m, 2H), 7.45–7.47 (m, 4H), 7.96 (d, 2H, $J = 7.8$ Hz), 8.05 (d, $J = 8.8$ Hz, 2H), 8.33 ppm (d, $J = 8.8$ Hz, 2H); ^{13}C NMR ($CDCl_3$, TMS, 100 MHz): $\delta = 10.39$, 22.42, 114.40, 114.45, 124.56, 126.50, 126.84, 127.81, 127.99, 128.91, 134.17, 134.29, 136.61, 147.21, 148.32, 161.21 ppm; HRMS (FAB+): *m/z* calcd for $[C_{36}H_{28}N_4O_2+H]^+$: 548.2291; found: 548.2289; elemental analysis calcd (%) for $C_{36}H_{28}N_4O_2$: C 78.81, H 5.14, N 10.21; found: C 78.60, H 5.10, N 9.96.

Compound 2

According to the method employed for synthesis of **1**, compound **2** was obtained from Azo precursor (1.01 mmol) and 1,5-dibromopentane (yield: 1.21 mmol, 21%). ^{1}H NMR ($CDCl_3$, TMS, 400 MHz): $\delta = 1.33$ (quint., $J = 8.0$ Hz, 2H), 1.44–1.53 (m, 2H), 1.67–1.78 (m, 2H), 3.93–3.99 (m, 2H), 4.17–4.23 (m, 2H), 6.57 (d, $J = 8.8$ Hz, 4H), 7.21–7.25 (m, 2H), 7.28–7.32 (m, 6H), 7.45–7.49 (m, 2H), 7.95 (d, $J = 8.3$ Hz, 2H), 8.05 (d, $J = 9.3$ Hz, 2H), 8.33 ppm (d, $J = 9.3$ Hz, 2H); ^{13}C NMR ($CDCl_3$, TMS, 100 MHz): $\delta = 22.11$, 28.80, 67.71, 115.44, 115.55, 125.02, 126.35, 126.72, 128.05, 128.56, 129.10, 134.28, 134.36, 146.37, 148.94, 160.66 ppm (unfortunately, one peak could not be detected due to signal overlapping or poor signal-to-noise in the ^{13}C NMR spectrum); HRMS (FAB+): *m/z* calcd for $[C_{37}H_{30}N_4O_2+H]^+$: 562.2447; found: 562.2448; elemental analysis calcd (%) for $C_{37}H_{30}N_4O_2$: C 78.98, H 5.37, N 9.96; found: C 78.74, H 5.38, N 9.80.

Compound 3

According to the method employed for synthesis of **1**, compound **3** was obtained from Azo precursor (2.43 mmol) and 1,6-dibromohexane (yield: 2.92 mmol, 20%). ^{1}H NMR ([D$_6$]DMSO, TMS, 400 MHz): $\delta = 1.18$–1.26 (m, 4H), 1.39–1.42 (m, 2H), 1.50–1.58 (m, 2H), 4.00–4.06 (m, 2H), 4.16–4.22 (m, 2H), 6.72 (d, $J = 9.8$ Hz, 4H), 7.20 (d, $J = 8.8$ Hz, 2H), 7.23 (d, $J = 8.8$ Hz, 4H), 7.36 (t, $J = 7.8$ Hz, 2H), 7.58 (t, $J = 6.8$ Hz, 2H), 8.12 (d, $J = 8.8$ Hz, 2H), 8.23 ppm (s, 4H); ^{13}C NMR ($CDCl_3$, TMS, 100 MHz): $\delta = 23.80$, 27.59, 66.99, 115.37, 115.44, 124.82, 126.36, 126.72, 128.09, 128.52, 129.12, 134.21, 134.38, 146.48, 148.93, 160.14 ppm (unfortunately, one peak could not be detected due to signal overlapping or poor signal-to-noise in the ^{13}C NMR spectrum); HRMS (FAB+): *m/z* calcd for $[C_{38}H_{32}N_4O_2+H]^+$: 577.2604; found: 577.2605; elemental analysis calcd (%) for $C_{38}H_{32}N_4O_2$: C 79.14, H 5.59, N 9.72; found: C 79.07, H 5.63, N 9.58.

Compound 4

According to the method employed for synthesis of **1**, compound **4** was obtained from Azo precursor (1.01 mmol) and 1,7-dibromoheptane (yield: 1.06 mmol, 50%). ^{1}H NMR ($CDCl_3$, TMS, 400 MHz): $\delta = 1.51$–1.61 (m, 6H), 4.00–4.06 (m, 4H), 4.11–4.17 (m, 4H), 6.66 (d, $J = 8.8$ Hz, 4H), 7.23–7.27 (m, 2H), 7.32 (d, $J = 8.8$ Hz, 4H), 7.38 (d, $J = 8.3$ Hz, 2H), 7.48 (m, 2H), 7.96 (d, $J = 8.3$ Hz, 2H), 8.05 (d, $J = 9.3$ Hz, 2H), 8.25 ppm (d, $J = 9.3$ Hz, 2H); ^{13}C NMR ($CDCl_3$, TMS, 100 MHz): $\delta = 24.71$, 27.94, 28.08, 67.51, 115.26, 115.29, 124.68, 126.39, 126.74, 128.12, 128.39, 129.13, 134.05, 134.37, 134.57, 146.68, 148.88, 160.35 ppm; HRMS (FAB+): *m/z* calcd for $[C_{39}H_{34}N_4O_2+H]^+$: 591.2760; found: 591.2761; elemental analysis calcd (%) for $C_{39}H_{34}N_4O_2$: C 79.30, H 5.80, N 9.48; found: C 79.10, H 5.92, N 9.27.

Compound 5

According to the method employed for synthesis of **1**, compound **5** was obtained from Azo precursor (1.01 mmol) and 1,8-dibromooctane (yield: 1.21 mmol, 27%). ^{1}H NMR ($CDCl_3$, TMS, 400 MHz): $\delta = 1.17$–1.25 (m, 4H), 1.30–1.37 (quint., $J = 6.8$ Hz, 4H), 1.59–1.65 (quint., $J = 6.8$ Hz, 4H), 3.90–4.04 (m, 2H), 4.07–4.13 (m, 2H), 6.65

(d, J=9.3 Hz, 4H), 7.24–7.27 (m, 2H), 7.31 (d, J=9.3 Hz, 4H), 7.41 (d, J=8.0 Hz, 2H), 7.47–7.51 (m, 2H), 7.97 (d, J=7.8 Hz, 2H), 8.04 (d, J=9.3 Hz, 2H), 8.19 ppm (d, J=8.8 Hz, 2H); ^{13}C NMR ($CDCl_3$, TMS, 100 MHz); δ=24.87, 27.58, 27.82, 67.44, 114.93, 115.38, 124.68, 126.38, 126.67, 128.14, 128.14, 129.13, 133.91, 134.29, 134.32, 146.68, 149.16, 160.57 ppm; HRMS (FAB+): m/z calcd for $[C_{40}H_{36}N_4O_2+H]^+$: 605.2917; found: 605.2918; elemental analysis calcd (%) for $C_{40}H_{36}N_4O_2$: C 79.48, H 6.05, N 9.09; found: C 79.44, H 6.00, N 9.26.

Compound 6

Azo precursor (200 mg, 0.40 mmol), K_2CO_3 (335 mg, 2.42 mmol), iodomethane (344 mg, 2.42 mmol), and DMF (20 mL) were added to a flask (50 mL). The mixture was stirred at 70 °C for 3 h. After distilled water was added to the resulting mixture to dissolve residual K_2CO_3, the solution was extracted with Et_2O, washed with distilled water, dried over Na_2SO_4, filtered, and then evaporated. The residue was purified by using column chromatography on silica gel with hexane/DCM (3:7) as the eluent to afford **6** as an orange amorphous solid (yield: 168 mg, 80%). ^{1}H NMR ([D$_6$]DMSO, TMS, 400 MHz): δ=3.73 (s, 6H), 6.89 (d, J=9.7 Hz, 4H), 7.25 (d, J=8.8 Hz, 4H), 7.28 (t, J=8.8 Hz, 2H), 7.38 (t, J=6.8 Hz, 2H), 7.59 (t, J=7.8 Hz, 2H), 8.09 (d, J=8.8 Hz, 2H), 8.13 (d, J=7.8 Hz, 2H), 8.21 ppm (d, J=8.8 Hz, 2H); ^{13}C NMR ($CDCl_3$, TMS, 100 MHz): δ=55.41, 113.88, 114.41, 124.57, 126.54, 26.89, 127.81, 128.01, 128.94, 129.46, 134.19, 136.46, 147.35, 148.29, 161.56 ppm; HRMS (FAB+): m/z calcd for $[C_{34}H_{26}N_4O_2+H]^+$: 523.2134; found: 523.2134; elemental analysis calcd (%) for $C_{34}H_{26}N_4O_2$: C 78.14, H 5.01, N 10.72; found: C 78.09, H 5.19, N 10.57.

Compound 7

According to the method employed for synthesis of **6**, compound **7** was obtained from Azo precursor (0.30 mmol) and 1-bromopropane (yield: 2.43 mmol, 81%); ^{1}H NMR ([D$_6$]DMSO, TMS, 400 MHz): δ=0.91 (t, J=7.3 Hz, 6H), 1.62–1.71 (m, 4H), 3.90 (t, J=6.8 Hz, 4H), 6.87 (d, J=8.8 Hz, 4H), 7.24 (d, J=9.3 Hz, 2H), 7.28 (d, J=8.3 Hz, 2H), 7.38 (t, J=7.3 Hz, 2H), 7.59 (t, J=7.8 Hz, 2H), 8.09 (d, J=9.3 Hz, 2H), 8.13 (d, J=8.3 Hz, 2H), 8.21 ppm (d, J=8.8 Hz, 2H); ^{13}C NMR ($CDCl_3$, TMS, 100 MHz): δ=10.39, 22.42, 69.65, 114.40, 114.45, 124.56, 126.50, 126.84, 127.81, 127.99, 128.91, 134.17, 134.29, 136.61, 147.21, 148.23, 161.21 ppm; HRMS (FAB+): m/z calcd for $[C_{38}H_{34}N_4O_2+H]^+$: 579.2760; found: 579.2759; elemental analysis calcd (%) for $C_{38}H_{34}N_4O_2$: C 78.87, H 5.95, N 9.61; found: C 78.87, H 5.92, N 9.68.

Evaluation of Photochemical Isomerization in Solution

Photochemical isomerization of chiral dopants in MeCN was carried out under visible-light irradiation in a 1 cm quartz cell with stirring by a magnetic stirrer. The photostationary state was assessed by monitoring until there were no more UV/Vis spectral changes after light irradiation.

Measurement of Helical Pitch and Handness

The helical pitch of the samples was determined by using a typical Grandjean–Cano wedge method.[44] The LC mixture was injected into a wedge cell (E.H.C. Co., KCRK-07, $\tan\theta$=0.0079) and then the Cano line was observed by using a POM. The helical pitch of N* was determined according to Equation (3):

$$p = 2L\tan\theta \quad (3)$$

in which L is the distance between the Cano lines and θ represents the wedge angle of the wedge cell. The helical twisting power (HTP) was calculated by using Equation (2).

The helical sense was determined by using the contact method.[44] A sample and cholesteryl oleyl carbonate (COC) were introduced from each side into the wedge cell by capillary effect and then the miscibility of both materials was observed by using a POM. If both materials have same helical sense, the Cano lines are continuous throughout the contact region, which indicates that the LC mixture has a left-handed helicity because COC exhibits left-handed N*. Conversely, discontinuous Cano lines and the appearance of a nematic phase between two materials indicate that the helix of the sample is right-handed. As is customary, the right- and left-handed helical senses of N* are represented as positive (+) and negative (−), respectively.

POM Observation with Circular Polarized Light Films

All images were captured by using a POM (Axio Imager.A2, Carl Zeiss MicroImaging) equipped with a EMCCD camera (Rolera EM-C^2 with a silica glass, Roper Technologies), a RGB color filter module (RGB-HM-S-IR type, Roper Technologies) and a filter slider (homemade in our laboratory), in reflection mode. Left- and right-handed CPL films (CP125L and CP125R, MeCan Imaging, 1/4λ film (125 nm retardation)) were attached to the handmade filter slider. For details of the apparatuses used, see Figure S7.

Acknowledgements

The authors thank K. Rijeesh (Institute for Material Chemistry and Engineering, Kyushu University) for valuable comments and advice. This work was partially supported by a Grant-in-Aid for Scientific Research (A) JSPS KAKENHI (grant number JP25248021) from the Japan Society for the Promotion of Science and Dynamic Alliance for Open Innovation Bridging Human, Environment and Materials from the Ministry of Education, Culture, Sports, Science and Technology (MEXT), Japan, and CREST, JST (JPMJCR1424). The authors would like to thank Enago (www.enago.jp) for the English language review.

Conflict of Interest

The authors declare no conflict of interest.

Keywords: azo compounds · binaphthyl · chirality · isomerization · liquid crystals · selective reflection

[1] H. S. Kitzerow, C. Bahr, in *Chirality in Liquid Crystals* (Eds.: H.-S. Kitzerow, C. Bahr), Springer, New York, **2001**, Chapter 1.
[2] A. Y. Bobrovsky, V. P. Shibaev, *Adv. Funct. Mater.* **2002**, *12*, 367–372.
[3] R. A. van Delden, T. Mecca, C. Rosini, B. L. Feringa, *Chem. Eur. J.* **2004**, *10*, 61–70.
[4] Q. Li, L. Green, N. Venkataraman, I. Shiyanovskaya, A. Khan, A. Urbas, J. W. Doane, *J. Am. Chem. Soc.* **2007**, *129*, 12908–12909.
[5] T. J. White, R. L. Bricker, L. V. Natarajan, N. V. Tabiryan, Q. Li, T. J. Bunning, *Adv. Funct. Mater.* **2009**, *19*, 3484–3488.
[6] M. Mathews, R. S. Zola, S. Hurley, D.-K. Yang, T. J. White, T. J. Bunning, Q. Li, *J. Am. Chem. Soc.* **2010**, *132*, 18361–18366.

[7] R. Thomas, Y. Yoshida, T. Akasaka, N. Tamaoki, *Chem. Eur. J.* **2012**, *18*, 12337 – 12348.
[8] Y. Wang, A. Urbas, Q. Li, *J. Am. Chem. Soc.* **2012**, *134*, 3342 – 3345.
[9] Y. Li, A. Urbas, Q. Li, *J. Am. Chem. Soc.* **2012**, *134*, 9573 – 9576.
[10] L. Wang, H. Dong, Y. Li, C. Xue, L.-D. Sun, C.-H. Yan, Q. Li, *J. Am. Chem. Soc.* **2014**, *136*, 4480 – 4483.
[11] J. Fan, Y. Li, H. K. Bisoyi, R. S. Zola, D. Yang, T. J. Bunning, D. A. Weitz, Q. Li, *Angew. Chem. Int. Ed.* **2015**, *54*, 2160 – 2164; *Angew. Chem.* **2015**, *127*, 2188 – 2192.
[12] Z. Zheng, Y. Li, H. K. Bisoyi, L. Wang, T. J. Bunning, Q. Li, *Nature* **2016**, *531*, 352 – 356.
[13] L. Wang, Q. Li, *Adv. Funct. Mater.* **2016**, *26*, 10 – 28.
[14] X. Chen, L. Wang, Y. Chen, C. Li, G. Hou, X. Liu, X. Zhang, W. He, H. Yang, *Chem. Commun.* **2014**, *50*, 691 – 694.
[15] G. Chen, L. Wang, Q. Wang, J. Sun, P. Song, X. Chen, X. Liu, S. Guan, X. Zhang, L. Wang, H. Yang, H. Yu, *ACS Appl. Mater. Interfaces* **2014**, *6*, 1380 – 1384.
[16] L. Wang, H. Dong, Y. Li, R. Liu, Y.-F. Wang, H. K. Bisoyi, L.-D. Sun, C.-H. Yan, Q. Li, *Adv. Mater.* **2015**, *27*, 2065 – 2069.
[17] Y.-H. Lee, L. Wang, H. Yang, S.-T. Wu, *Opt. Express* **2015**, *23*, 22658 – 22666.
[18] E. Montbach, N. Venkataraman, J. W. Doane, A. Khan, G. Magyar, I. Shiyanovskaya, T. Schneider, L. Green, Q. Li, *SID Dig. Tech. Pap.* **2008**, *39*, 919 – 922.
[19] N. Venkataraman, G. Magyar, E. Montbach, A. Khan, T. Schneider, J. W. Doane, L. Green, Q. Li, *J. Soc. Inf. Disp.* **2009**, *17*, 869 – 873.
[20] A. Bobrovsky, V. Shibaev, *J. Mater. Chem.* **2009**, *19*, 366 – 372.
[21] Y. Inoue, H. Yoshida, K. Inoue, Y. Shiozaki, H. Kubo, A. Fujii, M. Ozaki, *Adv. Mater.* **2011**, *23*, 5498 – 5501.
[22] J. Chen, S. M. Morris, T. D. Wilkinson, H. J. Coles, *Appl. Phys. Lett.* **2007**, *91*, 121118.
[23] C. A. Bailey, V. P. Tondiglia, L. V. Natarajan, M. M. Duning, R. L. Bricker, R. L. Sutherland, T. J. White, M. F. Durstock, T. J. Bunning, *J. Appl. Phys.* **2010**, *107*, 013105.
[24] T. J. White, R. L. Bricker, L. V. Natarajan, V. P. Tondiglia, C. Bailey, L. Green, Q. Li, T. J. Bunning, *Opt. Commun.* **2010**, *283*, 3434 – 3436.
[25] N. Tamaoki, A. V. Purfenov, A. Masaki, H. Matsuda, *Adv. Mater.* **1997**, *9*, 1102 – 1104.
[26] Y. Huang, Y. Zhou, C. Doyle, S.-T. Wu, *Opt. Express* **2006**, *14*, 1236 – 1242.
[27] L. V. Natarajan, J. M. Wofford, V. P. Tondiglia, R. L. Sutherland, H. Koerner, R. A. Vaia, T. J. Bunning, *J. Appl. Phys.* **2008**, *103*, 093107.
[28] S. Furumi, N. Tamaoki, *Adv. Mater.* **2010**, *22*, 886 – 891.
[29] L. Zhang, L. Wang, U. S. Hiremath, H. K. Bisoyi, G. G. Nair, C. V. Yelamaggad, A. M. Urbas, T. J. Bunning, Q. Li, *Adv. Mater.* **2017**, *29*, 1700676.
[30] S. M. Morris, P. J. M. Hands, S. Findeisen-Tandel, R. H. Cole, T. D. Wilkinson, H. J. Coles, *Opt. Express* **2008**, *16*, 18827.
[31] M. Mitov, N. Dessaud, *Nat. Mater.* **2006**, *5*, 361 – 364.
[32] N. A. Ha, Y. Ohtsuka, S. M. Jeong, S. Nishimura, G. Suzaki, Y. Takanishi, K. Ishikawa, H. Takezoe, *Nat. Mater.* **2008**, *7*, 43 – 47; S. M. Jeong, S. Nishimura, G. Suzaki, Y. Takanishi, K. Ishikawa, H. Takezoe, *Nat. Mater.* **2008**, *7*, 43 – 47.
[33] G. Gottarelli, M. Hibert, B. Samori, G. Solladié, G. P. Spada, R. Zimmermann, *J. Am. Chem. Soc.* **1983**, *105*, 7318 – 7321.
[34] G. Gottarelli, G. P. Spada, R. Bartsch, G. Solladié, R. Zimmermann, *J. Org. Chem.* **1986**, *51*, 589 – 592.
[35] C. Rosini, I. Rosati, G. P. Spada, *Chirality* **1995**, *7*, 353 – 358.
[36] A. Ferrarini, G. J. Moro, P. L. Nordio, *Liq. Cryst.* **1995**, *19*, 397 – 399.
[37] A. Ferrarini, G. J. Moro, P. L. Nordio, *Phys. Rev. E* **1996**, *53*, 681 – 688.
[38] S. F. Mason, R. H. Seal, D. R. Seal, *Tetrahedron* **1974**, *30*, 1671.
[39] L. D. Bari, G. Pescitelli, P. Salvadori, *J. Am. Chem. Soc.* **1999**, *121*, 7998 – 8004.
[40] N. Berova, L. D. Bari, G. Pescitellib, *Chem. Soc. Rev.* **2007**, *36*, 914 – 931.
[41] G. Heppke, F. Oestreicher, *Mol. Cryst. Liq. Cryst. Lett. Sect.* **1978**, *41*, 245 – 249.
[42] K. Kakisaka, H. Higuchi, Y. Okumura, H. Kikuchi, *Chem. Lett.* **2014**, *43*, 624 – 625.
[43] W. R. Busing, *J. Am. Chem. Soc.* **1982**, *104*, 4829 – 4836.
[44] I. Dierking, *Textures of Liquid Crystals*, Wiley-VCH, Weinheim, **2003**.
[45] S. Pieraccini, G. Gottarelli, R. Labruto, S. Masiero, O. Pandoli, G. P. Spada, *Chem. Eur. J.* **2004**, *10*, 5632 – 5639.

Received: June 23, 2017
Version of record online September 5, 2017

